Operational Band-to-Band Correction and Attitude Refinement of Pelican-2: Dual-Panchromatic Attitude Restitution and Selective Bundle Adjustment with Preliminary Application to Earthquake Displacement and DEM Generation

Saif Aati, Antonio Martos, Eric L. Peters, Frank Warmerdam, Graham Mills, Adam Weber, Luna Gray, Minh Radel

Planet Labs PBC, San Francisco, CA, USA – saif.aati@planet.com

Keywords: Pelican constellation, band-to-band registration, bundle adjustment, satellite attitude dynamics, digital surface models, earthquake monitoring

Abstract

The Pelican satellite constellation, first launched by Planet Labs in 2025, continues the high-resolution imaging capability established by the SkySat program. The change to pushbroom sensors in Pelican presents new geometric challenges: satellite attitude variations and platform instabilities during acquisitions can produce band misregistration and geolocation errors that degrade downstream products. This paper presents an operational workflow developed for Pelican imagery, validated on Pelican-2, a technology demonstration satellite. The approach exploits the dual-panchromatic focal plane configuration to independently measure satellite wobble to greater accuracy than on onboard attitude sensors, combined with selective bundle adjustment and B-spline spatial correction to achieve sub-pixel band alignment without dense ground control points. Validation on 963 Pelican-2 scenes demonstrates sub-pixel band-to-band registration accuracy (RMSE < 0.12 px) and 4 m CE90 geolocation accuracy. Applications illustrate the potential for operational geoscience workflows: earthquake surface displacement mapping of the March 2025 Myanmar M7.7 rupture detects 4.0 m co-seismic offsets on the Sagaing Fault with minimal post-processing, and digital surface model generation from an opportunistic multi view acquisition yields preliminary elevation products free of jitter artifacts, demonstrating operational feasibility for constellation-scale processing.

1. Introduction

High-resolution multispectral Earth observation systems employing pushbroom imaging face fundamental challenges in achieving geometric accuracy and precise band-to-band (B2B) registration due to satellite attitude variations and platform instabilities during image acquisition (Poli and Toutin, 2012; Teshima and Iwasaki, 2008). Unlike frame cameras that capture instantaneous images, pushbroom sensors acquire data line by line as the satellite moves along its orbital path, making them inherently sensitive to fine attitude perturbations and mechanical vibrations, commonly referred to as jitter, originating from onboard subsystems such as reaction wheels, gyroscopes, and solar panels. These dynamic effects introduce geometric distortions that can degrade image quality, cause band misregistration, and reduce the accuracy of downstream products and applications including pansharpening, digital elevation model (DEM) generation, change detection, time-series analysis, and vegetation index computation.

Geometric distortions are particularly detrimental for machine learning and deep learning applications, where spatial inconsistencies in training data can significantly degrade model performance. (Elmes et al., 2020) reported classification accuracy reductions of 12–23% and confidence drops of up to 50% in the presence of co-registration errors. Applications requiring sub-pixel accuracy, such as earthquake displacement mapping (Avouac and Leprince, 2015), DEM extraction (Shean et al., 2016), and other geoscience applications cannot rely on standard off-the-shelf products. Reprocessing of basic-level data is often necessary to mitigate these errors and to remove geometric artifacts through advanced post-processing methods (Aati et al., 2022a, 2022b; Beaud et al., 2022).

Mitigation strategies can be broadly categorized into hardware- and image-processing-based approaches. Hardware solutions employ high-performance attitude sensors sampled above jitter frequencies, or auxiliary focal-plane sensors such as optical gyroscopes, to capture high-frequency perturbations (Janschek et al., 2005). While effective, these systems increase mission complexity and cost. In contrast, processing-based methods depend on dense, well-distributed ground control points (GCPs) for geometric correction and attitude refinement, conditions that are often difficult to meet consistently across different acquisition scenarios.

For band-to-band registration, conventional correction models typically rely on low-order polynomials or mesh-based transformations derived from inter-band tie points. Although computationally inexpensive, polynomial models cannot adequately capture non-linear orbital perturbations or the high-frequency attitude oscillations typical of agile satellites. On the other hand, mesh-based rubbersheeting approaches may amplify local errors in areas with sparse or uneven tie point distribution.

The Pelican satellite constellation, launched in 2025, exemplifies these challenges while also providing new opportunities for geometric performance enhancement. Designed as Planet Labs’ next-generation high-resolution imaging system, Pelican complements the existing SkySat fleet by bridging operational requirements between global coverage (PlanetScope) and targeted high-resolution observations. Generation-1 Pelican satellites feature an eight-band satellite comprising six multispectral (MS) and two panchromatic sensors, to create 50 cm ground sample distance ortho products. The dual-panchromatic configuration, with sensors offset along

This contribution has been peer-reviewed. The double-blind peer-review was conducted on the basis of the full paper.
https://doi.org/10.5194/isprs-annals-XI-1-2026-45-2026

and across-track by 1/2 pixel, allows for stacking that enhances signal-to-noise ratio and spatial resolution while enabling improved attitude determination and geometric calibration. This design supports sub-pixel attitude refinement through direct cross-correlation between the two panchromatic channels, providing also an intrinsic mechanism for continuous attitude monitoring and correction.

This study focuses on Pelican-2, a technology-demonstration satellite that serves as a validation platform for the operational Pelican constellation and provides an ideal testbed for developing and validating advanced methods for attitude refinement and band-to-band registration. The implemented framework characterizes and compensates satellite attitude to achieve sub-pixel registration accuracy, evaluated using data acquired by Pelican-2. Section 2 outlines the geometric correction methodology, Section 3 describes the dataset and presents the experimental results, and Section 4 demonstrates applications to Digital Surface Model (DSM) generation and geoscience analysis, followed by conclusions and future work in Section 5.

2. Methodology

The geometric correction workflow consists of three sequential phases (Figure 1): bias compensation, attitude refinement, and final bundle adjustment with spatial correction. Each phase incrementally improves the ancillary navigation and control (ANC) data toward a refined geometric model.

The first phase, bias compensation, establishes the initial geolocation by integrating on-orbit guidance, navigation, and control (GNC) data with a reference basemap to derive GCPs. Its main objectives are to quantify the initial pointing error and estimate systematic boresight bias components. Initial GCPs are extracted by matching the Pan2 reference band to an internal reference basemap (1 m resolution, ~5 m CE90 horizontal accuracy) using area-based correlation within a large search window. These broad search parameters accommodate the uncertainty in satellite-predicted pointing. The resulting offsets represent the difference between the on-orbit ANC-based geolocation and the ground truth, providing a baseline measure of geometric accuracy prior to refinement. In addition, this phase is executed iteratively across multiple scenes to characterize consistent, repeatable pointing offsets (boresight biases) that are intrinsic to the sensor–spacecraft geometry and independent of time-varying platform dynamics. This step forms part of the calibration phase and is monitored and revisited throughout the satellite’s operational lifespan to ensure continued alignment.

Building on the bias-compensated solution from Phase 1, Phase 2 refines the time-dependent attitude parameters to reduce geolocation errors induced by orbital dynamics and platform motion. Updated GCPs are collected using tighter search constraints and smaller matching windows, taking advantage of the improved pointing accuracy achieved in the previous phase. An updated reference DEM is incorporated to account for terrain effects, enabling more accurate ground intersection in areas with significant relief. Attitude parameters (roll, pitch, and yaw) are modeled as low-order polynomials whose coefficients are iteratively optimized to minimize GCP residuals. This parameterization captures the primary satellite dynamics while avoiding overfitting, which is essential given that GCPs are not always densely or evenly distributed across the scene. The resulting refined ANC provides improved geolocation accuracy and serves as the basis for the final refinement stage.

The third phase, bundle adjustment and spatial correction, addresses both time-dependent and spatially varying geometric distortions that remain after polynomial attitude refinement. A selective multi-band bundle adjustment is performed using three representative bands (Pan1, Pan2, and MS1). This configuration captures the full range of platform dynamics: Pan1 is sensitive to high-frequency perturbations, while MS1, positioned furthest from Pan2 on the focal plane, captures low-frequency variations. Attitude perturbations are modeled using cubic splines with knot spacing of approximately 100 image lines, enabling compensation for higher-frequency attitude variations that cannot be captured by the initial polynomial model. The spline-based refinement leverages dense inter-band tie point observations while remaining constrained by the ground control points and the polynomial solution from Phase 2. Knots are adjusted adaptively according to keypoints distribution.

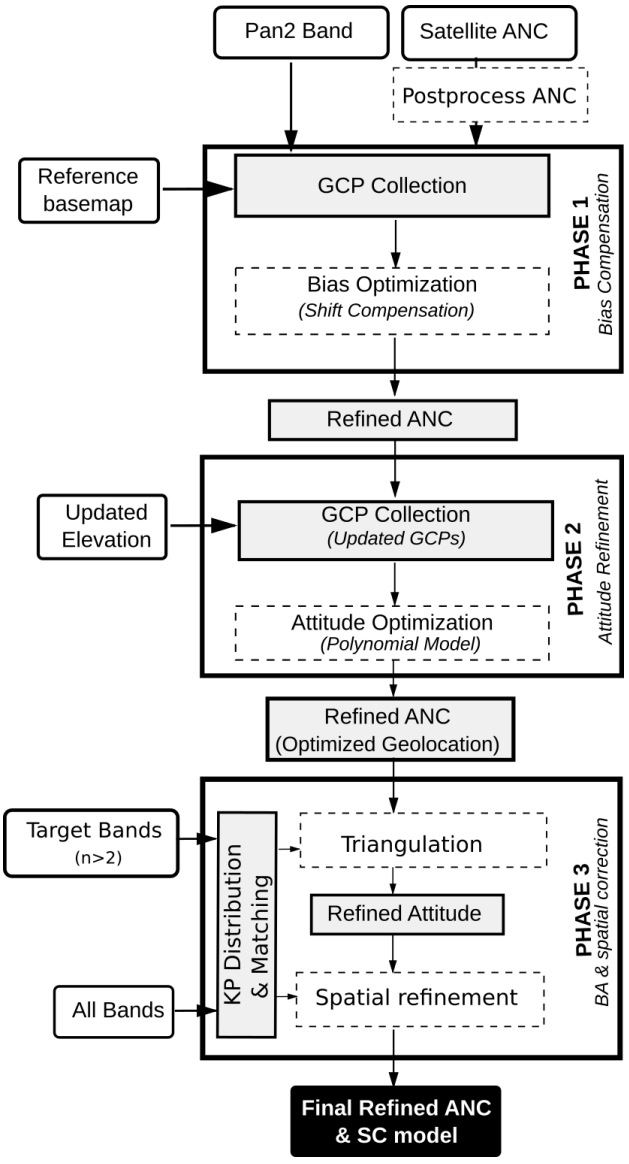

Figure 1. End to End workflow

Inter-band keypoints are identified through KP Distribution & Matching, an internally developed service based on area matching with FFT correlation, achieving ~1/20 pixel registration accuracy. Residual misalignments arising from

non-temporal, spatially varying geometric errors are subsequently corrected through pairwise spatial refinement. For each band relative to Pan2, corresponding features are matched and used to estimate a spatial B-spline correction model. Basis weights are determined by observation density within each basis, ensuring smooth transitions and robust performance over masked regions such as clouds and water bodies.

2.1 Attitude Restitution and Ancillary Data Postprocessing

A key advantage of the Pelican focal plane layout is its dual-panchromatic configuration, comprising Pan1 and Pan2 sensors with known physical offsets along the focal plane. The minimal parallax between these co-located panchromatic sensors, combined with their consistent radiometric properties, enables robust direct band-to-band correlation for attitude restitution. This geometric arrangement allows independent attitude measurement without relying on external reference data or dense ground control point networks. By exploiting the known physical separation between Pan1 and Pan2, along with their temporal acquisition offset during pushbroom scanning, it is possible to directly measure attitude-induced displacements in both along-track and cross-track directions. This approach isolates dynamic satellite motion from other geometric error sources, providing an independent reference of satellite dynamics decoupled from on-orbit GNC ancillary data.

This independent measurement capability is particularly important because Pelican employs low-cost MEMS (Micro-Electro-Mechanical Systems) gyroscopes and star sensors sampled at relatively low frequency. As discussed in the introduction, high-performance attitude sensors substantially increase mission cost and complexity. Consequently, these low-cost sensors cannot resolve high-frequency wobbles exceeding half the sampling rate (Ye et al., 2020), leaving high-frequency platform perturbations unobserved in standard GNC telemetry. By comparing our dual-panchromatic attitude restitution against GNC records, we directly assess ancillary data reliability, identify high-frequency components unresolved by MEMS sensors, and detect processing artifacts, thereby validating attitude information fidelity for geometric refinement

Figure 2-B illustrates an example of the radial error distribution between Pan1 and Pan2. The pattern clearly reveals satellite wobble, primarily manifested as quasi-periodic oscillations figure 2-A presents the error distribution map computed using standard on-orbit ancillary data (attitude quaternions and orbital ephemeris). Notable artifacts appear as discrete spatial discontinuities, including sharp jumps and steps inconsistent with satellite dynamics, resulting in up to ~1 pixel shift relative to Pan2 and ~12 pixels relative to MS1, the furthest band in the focal plane. These anomalies correspond to outliers or quantization errors in the telemetered ancillary data stream, which introduce artificial geometric distortions if used directly for image reconstruction.

To mitigate this issue, we developed a post-processing filter (Figure 1) that identifies and removes ancillary data outliers while preserving the underlying high-frequency attitude signal. Validation of this filtering approach is shown in Figure 2-C, which presents the error distribution after applying the post-processed ancillary data. The strong agreement between this result and the dual-panchromatic restitution (Figure 2-B) confirms that the filter effectively removes ancillary data artifacts while retaining genuine platform dynamics. Residual error patterns in both approaches now exhibit consistent spatial structure, dominated by along-track oscillations from satellite wobble. Figure 2-D quantifies this agreement through an extracted profile along the image track. The three profiles dual-pan restitution, raw on-orbit ancillary error, and post-processed ancillary error illustrate how the raw ancillary data contain significant excursions (orange profile) that are removed by post-processing (green profile), bringing it into close alignment with the independent restitution measurement (blue profile). The substantial reduction in error magnitude, particularly the elimination of the large negative excursions near pixel 7000, demonstrates the effectiveness of the filtering approach in restoring high-fidelity attitude information for geometric refinement.

3. Results

3.1 Dataset Overview

To evaluate the performance of the proposed workflow, we analyzed a comprehensive dataset acquired by the Pelican-2 technology demonstration satellite during its early operational phase. The analysis included 963 collects acquired between August 2, 2025, and October 13, 2025, all with cloud coverage below 10%. The selected collects cover diverse land cover types, including dense urban areas, mountainous terrain, and agricultural regions. This dataset also spans a wide range of acquisition geometries, with off-nadir angles from 0.1° to 32.3°, enabling a robust assessment of the workflow under varied satellite attitudes and viewing conditions typical of operational commercial imaging scenarios.

3.2 Band-to-Band Co-Registration Performance

To assess the performance of the proposed correction framework, we analyzed the along-track and cross-track error distributions throughout the four processing phases: (1) initial on-orbit ancillary data, (2) rectified ancillary data using GCPs only, (3) bundle-adjusted ancillary data based on three-band optimization, and (4) the final bundle-adjusted data combined with the spatial B-spline correction.

Figure 3 illustrates an example of the inter-band misalignment. The PAN1–PAN2 pair, selected to represent high-frequency attitude wobbles with minimal parallax sensitivity, and the PAN2–MS1 pair, reflecting low-frequency errors that are more sensitive to parallax and topography, were used to characterize the error spectrum. Using initial ancillary data, PAN1–PAN2 errors reached ~ 1 pixel, while PAN2–MS1 errors were ~ 5 pixels, corresponding to 1–15 m geolocation offsets at 50 cm GSD. These large discrepancies highlight the impact of uncorrected high- and low-frequency attitude perturbations.

The rectification phase using only GCPs showed negligible improvement in band-to-band, which was expected since the sparse GCP distribution and polynomial model cannot capture these time-dependent perturbations. After bundle adjustment, both high- and low-frequency components were substantially reduced to below 0.3 pixels, demonstrating an effective ability to compensate for tie-dependent attitude errors. Small spatially varying residuals ($\leq$ 0.3 pixels) that remained were fully mitigated by the subsequent B-spline correction. The combined approach achieved sub-0.1 pixel co-registration accuracy, meeting the mission’s $\leq$ 0.3 pixel RMS specification.
A visual example (Figure 4) demonstrates the improvement in multispectral composites: color fringes evident in uncorrected images, especially along building edges and terrain discontinuities, disappear after correction, resulting in crisp, well-aligned features

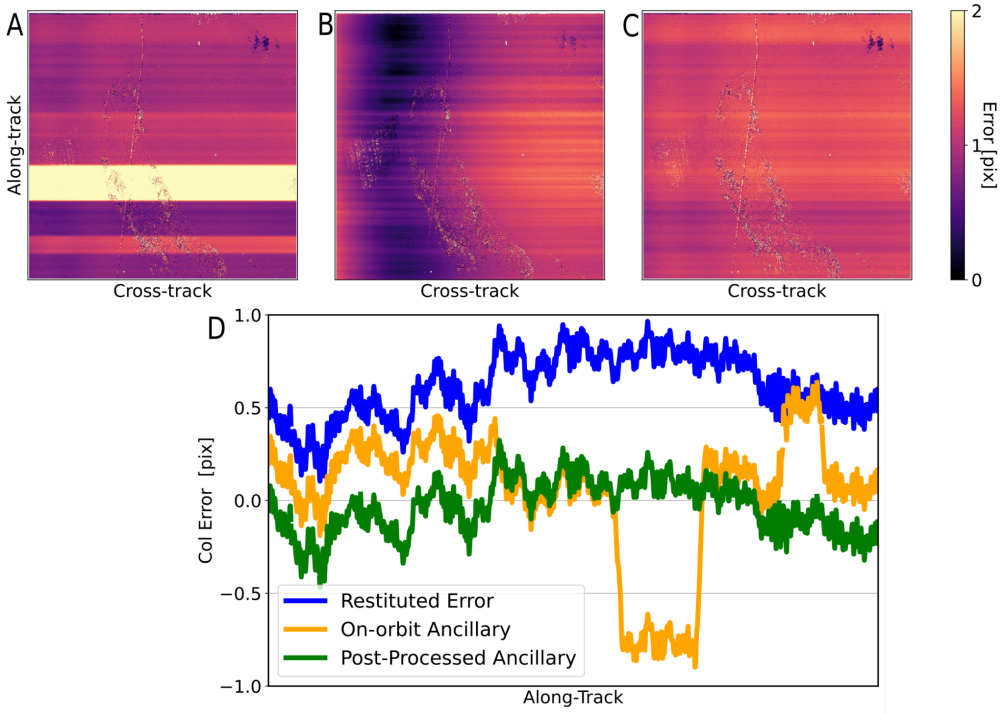

Figure 2. Attitude restitution and ancillary data validation for Pelican satellite imager

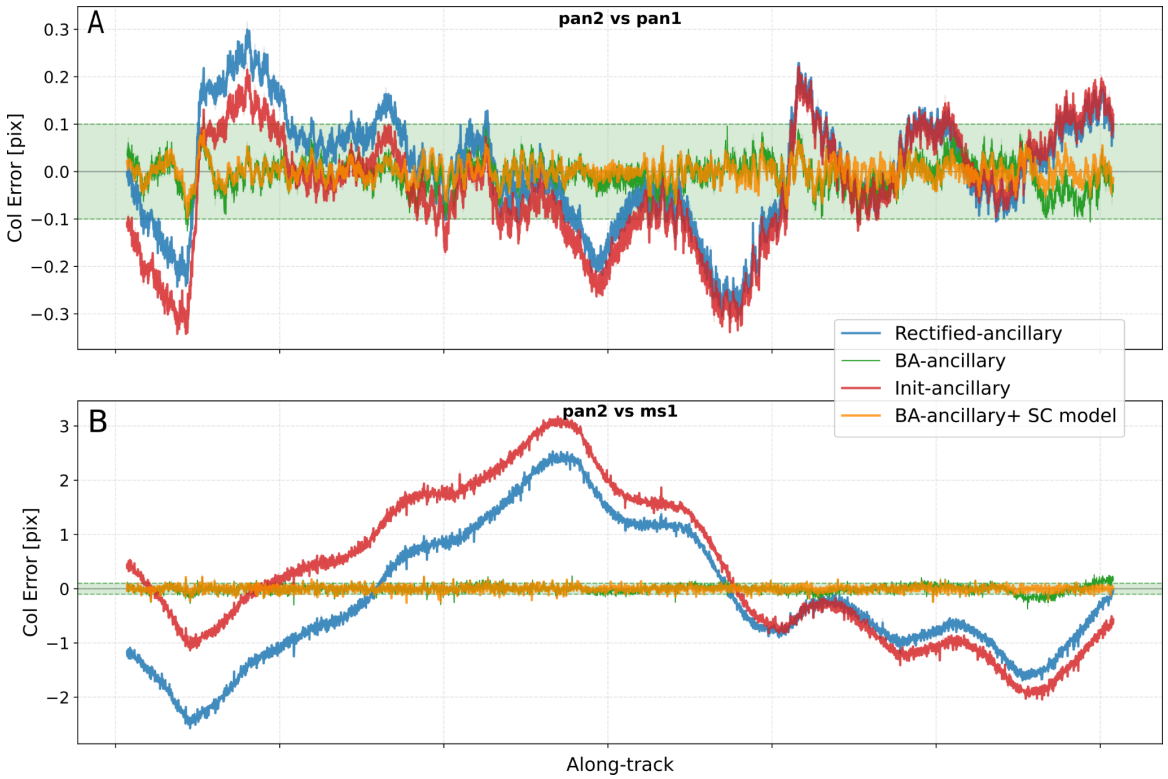

Figure 3. Band-to-band registration error across the four processing phases. Panel (A) shows the along-track error between the PAN1–PAN2 band pair, while Panel (B) presents the along-track error between PAN2–MS1.

This contribution has been peer-reviewed. The double-blind peer-review was conducted on the basis of the full paper.
https://doi.org/10.5194/isprs-annals-XI-1-2026-45-2026 | © Author(s) 2026. CC BY 4.0 License.

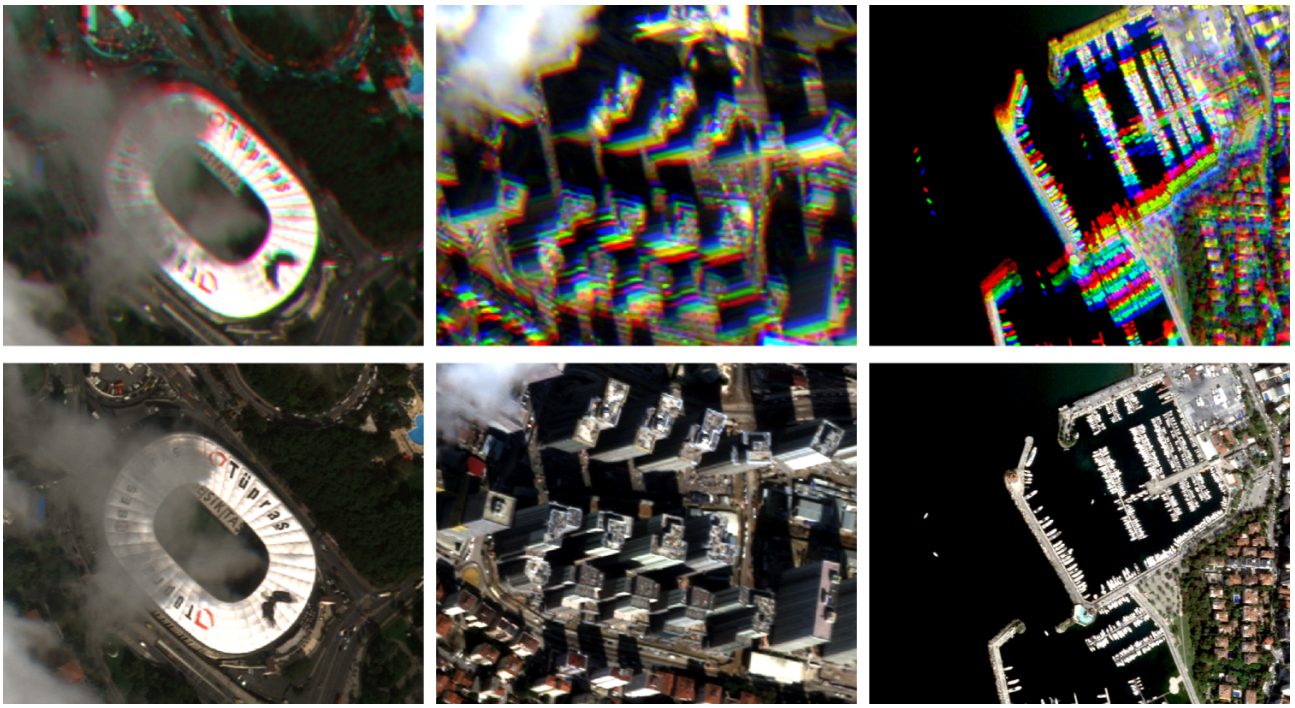

Figure 4. Multi-spectral band registration improvement. (Top row) Uncorrected Pelican-2 RGB composite imagery. (Bottom row) Imagery after correction.

Quantitative validation over all eight spectral bands (Figure 5) confirms stable sub-pixel accuracy, with mean RMSE values below 0.12 pixels. The Red Edge 1 band achieved the best accuracy (mean 0.070 pixels, median 0.068 pixels), while broader bands such as NIR Wide and Blue exhibited slightly higher errors (0.12–0.13 pixels). The low inter-band standard deviation (0.016–0.034 pixels) demonstrates consistent correction performance across scene types, viewing geometries, and illumination conditions, ensuring reliable image co-registration for downstream applications such as change detection and displacement mapping.

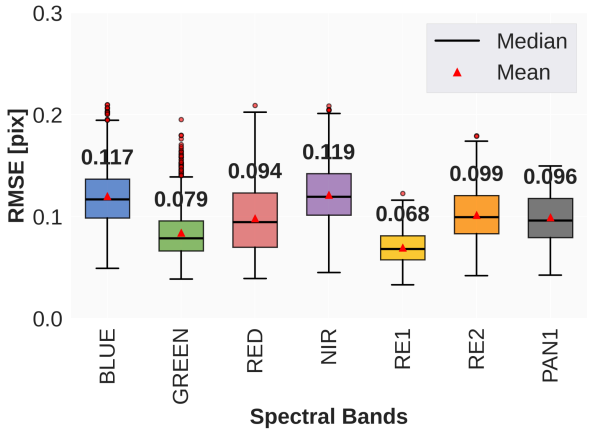

Figure 5. Band-to-band registration accuracy across all Pelican-2 spectral channels (n=962 scenes). Box plot showing RMSE distribution for each of the eight spectral bands after applying the proposed attitude refinement method. Red triangles indicate mean RMSE values; horizontal black lines show medians; boxes represent the inter-quartile range.

3.4 Geolocation

Beyond relative band-to-band registration, we evaluated geolocation accuracy before and after applying the refined workflow (cf., Figure 6). The initial geolocation error, assessed using the first phase of rectification of our workflow, following boresight alignment and camera calibration, provides a baseline for quantifying pointing errors and boresight misalignment. At this stage, relying solely on orbit ephemeris data and attitude information, the mean CE90 geolocation error was ~ 60 m.

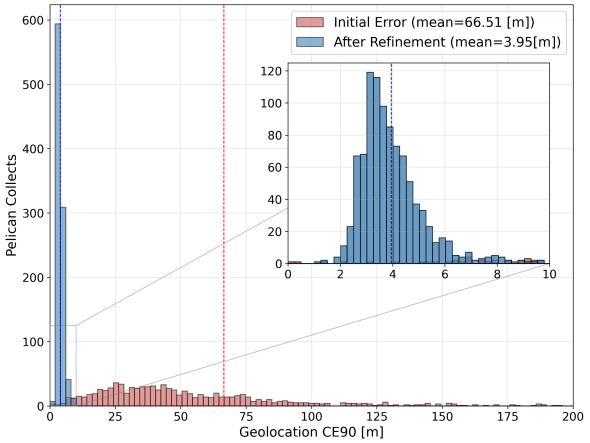

Figure 6. Geolocation accuracy performance. Histogram showing distribution of CE90 across 962 image scenes before (red) and after (blue) refinement. The inset detail shows the post-correction distribution.

After applying rectification and bundle-adjustment-based attitude refinement using selective three-band inputs, the

https://doi.org/10.5194/isprs-annals-XI-1-2026-45-2026

mean CE90 geolocation error was reduced to approximately 4 m—representing an improvement factor of roughly 15×. This level of accuracy meets our geolocation requirements. Importantly, this method minimizes reliance on GCPs by leveraging relative band-to-band information to mitigate satellite wobble effects.

This improvement confirms that the refined bundle adjustment parameters effectively correct both relative band misalignment and absolute attitude errors that degrade geolocation accuracy. Given that the area-based matching technique employed achieves ~1/10 pixel accuracy, the remaining 4 m error likely reflects residual unmodeled attitude variations, ephemeris uncertainties, or inaccuracies in reference imagery and DEM data. Some contributions may also arise from systematic optical distortions, which will require further refinement. As the mission matures, additional improvements in absolute geolocation accuracy are expected. Notably, scenes acquired over terrain with slopes <20° and off-nadir angles <30° generally demonstrated slightly better performance, consistent with the reduced geometric correction complexity under these favorable conditions.

4. Applications

To explore Pelican imagery's potential for geoscience applications, two case studies are presented: co-seismic displacement mapping and digital elevation model generation.

4.1 Earthquake Surface Displacement Measurement

The March 28, 2025, magnitude 7.7 earthquake in central Myanmar was selected to validate Pelican's sub-pixel displacement mapping capability. The rupture occurred along the Sagaing Fault, one of Southeast Asia's most active strike-slip systems, producing surface displacements exceeding 4 m along approximately 460 km (Antoine et al., 2025). The scale and clarity of the rupture make it a good target for demonstrating Pelican's potential for fault mechanics studies and seismic hazard assessment.

Co-seismic displacement was measured from SkySat archival imagery (March 17, 2022) and Pelican-2 imagery specifically tasked for post-event coverage (March 28, 2025), processed using the methodology in Section 2 without additional post-processing. Analysis focused on a representative portion of the surface rupture to evaluate Pelican's displacement-mapping capability. Displacement was estimated using two established algorithms widely applied in the geoscience community: MicMac (Rosu et al., 2015) and COSI-Corr (Aati, 2021; Leprince et al., 2007), which yielded consistent results. Figure 7 illustrates the north–south component of the surface displacement, with magnitudes reaching ~4.0 m. The results clearly delineate the fault trace, showing sharp offsets across the rupture. Profiles extracted perpendicular to the fault, Figure 7-B display the expected step-function signature typical of strike-slip earthquakes aligned with published study for the same event (Antoine et al., 2025).

The recovery of earthquake displacement from Pelican imagery, despite substantial temporal baselines, demonstrates notable advantages. The high geometric fidelity permits accurate displacement measurements without the extensive post-processing workflows often applied to other satellite high-resolution images (Aati et al., 2022a; Shean et al., 2016). While some residual low-frequency variations are observed in the displacement field, these do not compromise the primary objectives of fault mapping and displacement quantification. Moreover, the imagery is largely free from systematic distortions caused by CCD misalignment or attitude jitter, enabling direct use of orthorectified Pelican data with minimal post-processing. The observed low frequency wobble residuals will be investigated in future work, focusing on evaluating the performance of Pelican’s attitude refinement.

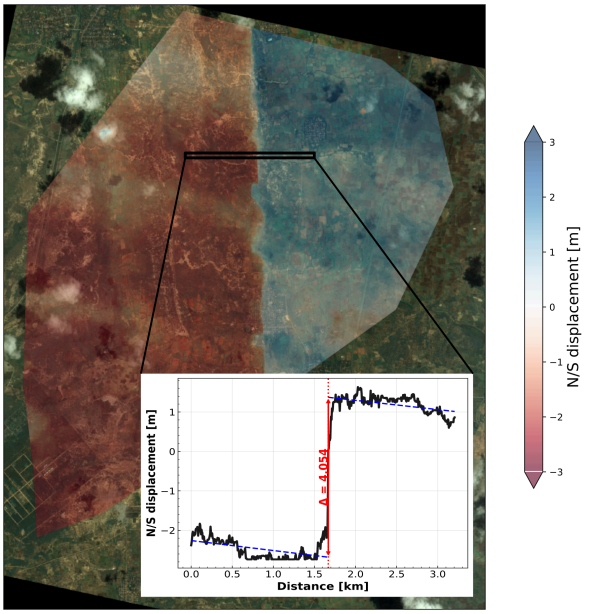

Figure 7. Surface co-seismic displacement map from the March 2025 Myanmar earthquake.

4.2 Pelican-2 Digital Surface Model Generation

A DSM extraction experiment was conducted using Pelican-2 imagery acquired during the satellite's initial operational phase, prior to full commissioning and payload calibration. This opportunistic assessment provided early validation of the satellite's multi-view photogrammetric processing capability.

After evaluating available cross-over collections, two collects over the Korean Peninsula (March 2025) were selected. The first was acquired at 512.7 km altitude with 28.7° off-nadir angle (westward, 284.2° azimuth), and the second at 511.9 km altitude with 10.8° off-nadir angle (eastward, 99.6° azimuth). This configuration yielded a convergence angle of 39.6° and base-to-height ratio of 0.826. The mountainous terrain with pronounced relief and diverse land cover provided a good testbed for 3D reconstruction.

The derived DSM shown in Figure 8 exhibits clear topographic definition, effectively capturing the complex relief patterns characteristic of the Korean Peninsula.

Notably, the absence of high-frequency striping artifacts indicates stable platform performance and effective attitude correction—jitter typically manifests as such artifacts in elevation models (Shean et al., 2016). Although the preliminary nature of these early acquisitions precluded rigorous absolute accuracy assessment, the results establish a baseline for operational DSM generation with Pelican-2.

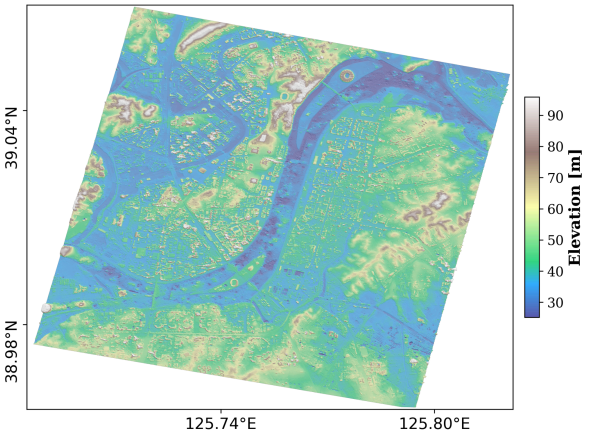

Figure 8. Digital Surface Model extracted from Pelican-2 multi view pair over Korean Peninsula.

5. Conclusion

This study validated the proposed geometric correction workflow for operational Pelican imagery using data from the Pelican-2 technology demonstration satellite. The three-phase approach, combining bias compensation, polynomial attitude refinement, and selective bundle adjustment with B-spline spatial correction, achieved mean band-to-band registration accuracy of ~0.1 pixels and geolocation accuracy of ~4 m CE90 across 963 validation scenes. Exploiting the dual-panchromatic focal plane configuration enabled independent measurement of satellite wobble, reducing dependence on dense ground control points and enhancing geometric stability for pushbroom systems. Preliminary applications, including earthquake surface displacement mapping of the March 2025 Myanmar M7.7 rupture and digital surface model generation, confirmed the workflow’s operational utility for precision geoscience. The consistent performance across diverse acquisition conditions demonstrates readiness for integration into production constellation operations.

Future work will extend this framework to constellation-scale validation as additional Pelican satellites become operational, enabling assessment of inter-satellite geometric consistency and long-term stability of refined attitude parameters. Further efforts will focus on quantitative evaluation of DSM accuracy through dedicated stereo campaigns and benchmarking against independent elevation data. Performance under challenging imaging conditions, such as high off-nadir viewing, steep terrain, and partial cloud cover, will also be systematically assessed. Finally, comparative analysis with other high-resolution constellations will support geometric interoperability and guide design improvements for next Pelican generation

References

Aati, S., Avouac, J.-P., Rupnik, E., Deseilligny, M.-P., 2022a. Potential and Limitation of PlanetScope Images for 2-D and 3-D Earth Surface Monitoring with Example of Applications to Glaciers and Earthquakes. IEEE Trans. Geosci. Remote Sens. 1–1. https://doi.org/10.1109/TGRS.2022.3215821

Aati, S., Milliner, C., Avouac, J.-P., 2022b. A new approach for 2-D and 3-D precise measurements of ground deformation from optimized registration and correlation of optical images and ICA-based filtering of image geometry artifacts. Remote Sens. Environ. 277, 113038. https://doi.org/10.1016/j.rse.2022.113038

Antoine, S.L., Shrestha, R., Milliner, C., Im, K., Rollins, C., Wang, K., Chen, K., Avouac, J.-P., 2025. The 2025 M_w 7.7 Mandalay, Myanmar, earthquake reveals a complex earthquake cycle with clustering and variable segmentation on the Sagaing Fault. Proc. Natl. Acad. Sci. 122, e2514378122. https://doi.org/10.1073/pnas.2514378122

Avouac, J.-P., Leprince, S., 2015. Geodetic Imaging Using Optical Systems, in: Treatise on Geophysics. Elsevier, pp. 387–424. https://doi.org/10.1016/B978-0-444-53802-4.00067-1

Beaud, F., Aati, S., Delaney, I., Adhikari, S., Avouac, J.-P., 2022. Surge dynamics of Shisper Glacier revealed by time-series correlation of optical satellite images and their utility to substantiate a generalized sliding law. The Cryosphere 16, 3123–3148. https://doi.org/10.5194/tc-16-3123-2022

Elmes, A., Alemohammad, H., Avery, R., Caylor, K., Eastman, J., Fishgold, L., Friedl, M., Jain, M., Kohli, D., Laso Bayas, J., Lunga, D., McCarty, J., Pontius, R., Reinmann, A., Rogan, J., Song, L., Stoynova, H., Ye, S., Yi, Z.-F., Estes, L., 2020. Accounting for Training Data Error in Machine Learning Applied to Earth Observations. Remote Sens. 12, 1034. https://doi.org/10.3390/rs12061034

Janschek, K., Tchernykh, V., Dyblenko, S., 2005. Integrated camera motion compensation by real-time image motion tracking and image deconvolution, in: Proceedings, 2005 IEEE/ASME International Conference on Advanced Intelligent Mechatronics. Presented at the 2005 IEEE/ASME International Conference on Advanced Intelligent Mechatronics., IEEE, Monterey, CA, pp. 1437–1444. https://doi.org/10.1109/AIM.2005.1511213

Leprince, S., Barbot, S., Ayoub, F., Avouac, J., 2007. Automatic and Precise Orthorectification, Coregistration, and Subpixel Correlation of Satellite Images, Application to Ground Deformation Measurements. IEEE Trans. Geosci. Remote Sens. 45, 1529–1558. https://doi.org/10.1109/TGRS.2006.888937

Poli, D., Toutin, T., 2012. Review of developments in geometric modelling for high resolution satellite pushbroom sensors: Geometric modelling for high resolution satellite pushbroom sensors. Photogramm. Rec. 27, 58–73. https://doi.org/10.1111/j.1477-9730.2011.00665.x

Rosu, A.-M., Pierrot-Deseilligny, M., Delorme, A., Binet, R.,

Klinger, Y., 2015. Measurement of ground displacement from optical satellite image correlation using the free open-source software MicMac. ISPRS J. Photogramm. Remote Sens., High-Resolution Earth Imaging for Geospatial Information 100, 48–59. https://doi.org/10.1016/j.isprsjprs.2014.03.002

Shean, D.E., Alexandrov, O., Moratto, Z.M., Smith, B.E., Joughin, I.R., Porter, C., Morin, P., 2016. An automated, open-source pipeline for mass production of digital elevation models (DEMs) from very-high-resolution commercial stereo satellite imagery. ISPRS J. Photogramm. Remote Sens. 116, 101–117. https://doi.org/10.1016/j.isprsjprs.2016.03.012

Teshima, Y., Iwasaki, A., 2008. Correction of Attitude Fluctuation of Terra Spacecraft Using ASTER/SWIR Imagery With Parallax Observation. IEEE Trans. Geosci. Remote Sens. 46, 222–227. https://doi.org/10.1109/TGRS.2007.907424

Ye, G., Pan, J., Zhu, Y., Jin, S., 2020. A JITTER DETECTION METHOD BASED ON THE INTEGRATION IMAGING MODEL. ISPRS Ann. Photogramm. Remote Sens. Spat. Inf. Sci. V-3–2020, 709–715. https://doi.org/10.5194/isprs-annals-V-3-2020-709-2020